JUSTC

Article

http://justc.ustc.edu.cn

Received: February 13, 2023; Accepted: April 30, 2023

Assessment study of different radiation models in the simulation of 1 m methanol pool fire

Qianjun Zhou, Yong Hu ✉, and Yong Jiang ✉

State Key Laboratory of Fire Science, University of Science and Technology of China, Hefei 230027, China

✉Correspondence: Yong Hu, E-mail: yhu18@ustc.edu.cn; Yong Jiang, E-mail: yjjiang@ustc.edu.cn

Graphical abstract

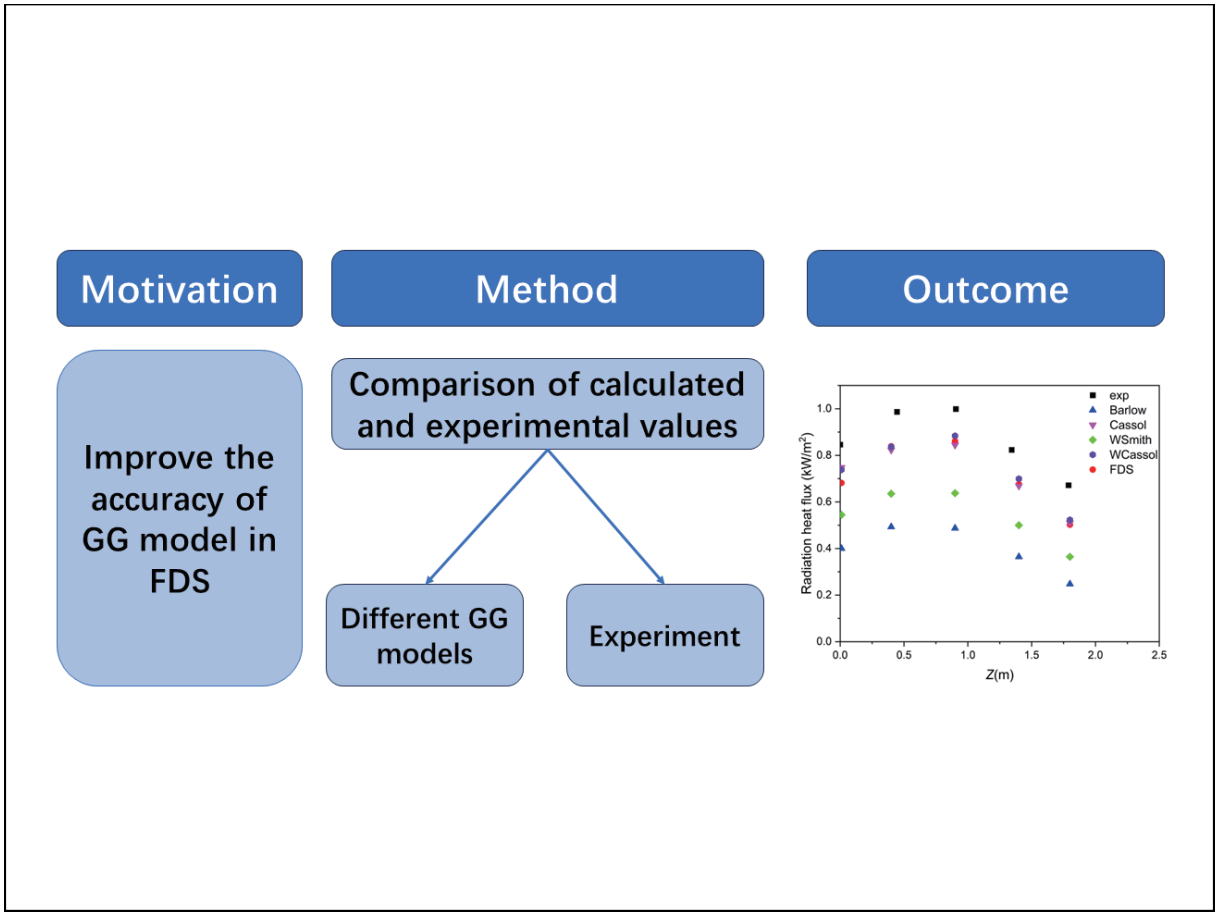

By comparing the improved models, the WCassol model and Cassol model have the best performance.

Public summary

- Based on the source code of FDS, different radiation model calculation modules have been developed for detailed large eddy simulations of pool fires. This provides a reference for the secondary development of the professional fire simulation program FDS.
- The performance and accuracy of different radiation models are evaluated, guiding for further improving the reliability of large-scale pool fire simulations.

Citation: Zhou Q J, Hu Y, Jiang Y. Assessment study of different radiation models in the simulation of 1 m methanol pool fire. *JUSTC*, **2023**, 53(10): 1005. DOI: 10.52396/JUSTC-2023-0021

JUSTC

Article

http://justc.ustc.edu.cn

Received: February 13, 2023; Accepted: April 30, 2023

Assessment study of different radiation models in the simulation of 1 m methanol pool fire

Qianjun Zhou, Yong Hu ✉, and Yong Jiang ✉

State Key Laboratory of Fire Science, University of Science and Technology of China, Hefei 230027, China

✉Correspondence: Yong Hu, E-mail: yhu18@ustc.edu.cn; Yong Jiang, E-mail: yjjiang@ustc.edu.cn

Cite This: *JUSTC*, **2023**, 53(10): 1005 (10pp)

Read Online

Abstract: Pool fires are one of the most commonly encountered flame types in fire disasters, and the accurate and detailed modeling of pool fires is beneficial for the hazard analysis and assessment of liquid-related fire accidents. The radiation model is known to be the critical component in the accurate simulation of various fire scenarios. Therefore, to develop a proper radiation model, an LES study of a large-scale methanol pool fire was performed in this work by coupling four different radiation models into the open-source fire simulation code FDS and solving the radiation intensity transport equation using the discrete ordinates method. The impact characteristics of different radiation models are evaluated in detail with the NIST experiments, where the comparative analysis was carried out. Regarding the temperature calculations, the WSGG (weighted-sum-of-gray-gases)-based radiation model and Cassol's model performed better. In addition, all models predict pulsation frequencies well. However, regarding the prediction of the radiative heat fluxes, Cassol's two models and the FDS default model outperformed the other models, which indicates that the database for obtaining the spectral information of each species and the method to determine the WSGG coefficient of mixed gases are significant factors for the successful prediction of flame radiation.

Keywords: pool fire; gray gas model; LES simulation; WSGG model

CLC number: TK121; X928.7 **Document code:** A

1 Introduction

Pool fires often occur when liquid fuel is accidentally spilled and ignited during fuel storage and transportation, and they can also induce a series of events that may amplify the hazards of the accident, leading to the well-known domino effect. The study has shown that 43% of domino accidents result initially from fire, and 80% of them are pool fires[1] and are dominated by radiation heat transfer[2, 3]. For liquid pool fires, the thermal feedback from flame radiation can, on the one hand, intensify fuel evaporation and thus increase the flame spreading area; on the other hand, it poses a significant threat to nearby fuel tanks and can potentially accelerate the development of fire[4]. Therefore, it is essential to establish reasonable models to account for the radiation heat transfer in pool fires.

However, a reliable calculation of gas radiation remains a challenging task, not only because of the difficulty in solving the radiation transport equation (RTE) but also because of the highly temperature-dependent radiation properties of the participating species (e.g., water, carbon dioxide, and soot) that emit and absorb thermal energy in the infrared part of the radiation spectrum, thus performing heat transfer. The approach in most studies[5–7] commonly adopts the assumption of a gray gas medium where the gaseous radiation properties are assumed to be constant at all wavelengths. This is also known as the GG (gray gas) model. Compared to the complex LBL (line-by-line) method, the GG model avoids the integration of radiation variations across hundreds of thousands of spectral lines and significantly reduces the computational cost. These advantages make the GG model favorable, especially in fire science, where radiation has to be solved along with large-scale fluid flow and turbulent combustion. Therefore, further improvement of the GG model's accuracy for various fire scenarios is the most desirable.

Hostikka et al.[8] evaluated the default GG model in the FDS (fire dynamics simulator) code, which is widely used in fire research, and found that the model can only qualitatively predict the pool size dependence of the burning rate. A similar observation was indicated by Ref. [9] in the simulation of a small-scale methane flame, where the results of default FDS's GG model were very close to those obtained by nongray calculations. Recently, Fernandes et al.[5] studied the modeling options for the evaluation of medium emittance in GG models by modeling small- to medium-scale pool fires. They found that the default formulation[10] in FDS can still provide a good prediction in the weekly sooting flames, although the evaluation method for medium emittance matters in determining the prediction accuracy. However, their work lacks an in-depth analysis of the difference between different modeling options, which is unbeneficial for the further improvement of GG models. Meanwhile, previous studies were limited to small pool fires, while large-scale fires are known to be more radiation-dominated.

DOI: 10.52396/JUSTC-2023-0021

JUSTC, **2023**, 53(10): 1005

Therefore, in this work, a large-eddy simulation of a 1 m large-scale methanol pool fire is carried out employing different modeling strategies for evaluating medium absorption properties. Compared to Ref. [5], WSGG (weighted-sum-of-gray-gases)-based models adopting different spectroscopic databases (i.e., HITEMP) and methods to evaluate mixture emittance are also investigated, along with a discussion of additional models for Planck-mean absorption coefficients. In total, five radiation models are considered, which are detailed in the next section. The purpose of this paper is to extend the FDS source code, and the program associated with all different radiation models is integrated into the source code to ensure that the fluid flow and combustion are solved with the same solvers. For a comprehensive parameter analysis, the in-house code is also developed to extract the various fire data from the FDS computations.

2 Numerical modeling

In this work, the modeling strategy for flame radiation is thoroughly evaluated in the large-eddy simulation of a 1 m diameter methanol pool fire[11]. Methanol fuel is chosen because the soot generation of methanol combustion is low, which can mitigate the coupling effect on radiation exchange due to soot and is beneficial to evaluate the accuracy of different models in predicting the more complex spectral dependence of the radiative coefficients of gas-phase species. This would eventually help to establish a theoretical basis for selecting a suitable radiation model to simulate various complex pool fires. The detailed data records in this experiment will help to validate the model.

2.1 Radiation models

The radiative transport equation (RTE) must be solved to obtain the radiation field. Since the heat dissipation albedo of submicron soot particles produced by hydrocarbon flames is very low, we generally ignore scattering in solving the RTE equation. Therefore, the RTE equation for a nonscattering gas under the GG model assumption with its spectrally integrated form can be written as[10]:

$$\frac{\mathrm{d}I}{\mathrm{d}s} = \kappa_\mathrm{m}(I_\mathrm{b} - I), \tag{1}$$

where I is the radiation intensity, I_b is the blackbody radiation intensity, and κ_m is the absorption coefficient of the gray-gas medium. In this paper, in addition to the use of the FDS default method to calculate κ_m, the other four GG models are employed by modification of the FDS source code. Generally, these five radiation models adopt different assumptions to determine the κ_m value that should have a highly complex spectral dependence for gaseous species. Below is a description of each model used.

Barlow's model[6] that calculates the gray gas absorption coefficient of each species by curve fitting the Planck-mean absorption coefficient from the narrow-band RADCAL database[12], and then the absorption coefficient for each species is given as:

$$\kappa_j = p_j \sum_{i=0}^{5} c_i \left(\frac{1000}{T}\right)^i, \tag{2}$$

where j represents the different species (e.g., H_2O, CO_2), p_j is the partial pressure, T is the temperature, and c_i is the polynomial fit coefficient. For the CO_2 -H_2O-soot mixture, its spectral absorption coefficient can be expressed as κ_m= $\kappa_{\mathrm{CO_2}}$+ $\kappa_{\mathrm{H_2O}}$+ κ_s. Here, the spectral absorption coefficient of soot κ_s is determined by Eq. (3), in which b_s=1864.32 $(\mathrm{m\cdot K\cdot atm})^{-1}$, f_v indicates the volume concentration of soot.

$$\kappa_\mathrm{s} = b_\mathrm{s} f_\mathrm{v} T. \tag{3}$$

Cassol's model[7] that fits the Planck-averaged absorption coefficient curves of water and carbon dioxide by using the latest spectral database HITEMP2010[13], and the species coefficient is therefore given by Eq. (4), where NP denotes the number of coefficients. The fitting coefficients in Eqs. (2) and (4) are shown in Table 1.

$$\kappa_j = \begin{cases} p_j \sum_{i=0}^{\mathrm{NP}} c_i T^i, & \kappa_{\mathrm{CO_2}} \text{ and } \kappa_{\mathrm{H_2O}}; \\ b f_\mathrm{v} \sum_{i=0}^{\mathrm{NP}} c_i T^i, & \kappa_\mathrm{s}. \end{cases} \tag{4}$$

Smith's WSGG-based model[14], Instead of curve-fitting the Planck average absorption coefficient, this method obtains the gray gas κ_m through the total emissivity (ε_m) of the gas mixture that is calculated by the WSGG-based model and Bouguer's formula,

$$\kappa_\mathrm{m} = -\frac{\ln(1-\varepsilon_\mathrm{m})}{S}, \tag{5}$$

where S denotes the optical path length. The emissivity fitted by Smith's model is derived from the data provided by the exponential broad-band model and can be written as:

Table 1. Polynomial fit coefficients used in Barlow and Cassol's models.

	Barlow[6]		Cassol[7]		
	CO_2	H_2O	CO_2	H_2O	Soot
c_0	1.8741×10^{1}	-2.3093×10^{-1}	-6.4750×10^{-1}	7.5702×10^{-1}	-2.8119×10^{-2}
c_1	-1.2131×10^{2}	1.1239	4.2895×10^{-3}	-1.9716×10^{-3}	3.7161
c_2	2.7350×10^{2}	9.4153	-6.6089×10^{-6}	2.1998×10^{-6}	-6.7737×10^{-4}
c_3	-1.9405×10^{2}	−2.9988	4.4190×10^{-9}	-1.2492×10^{-9}	
c_4	5.6310×10^{2}	5.1382×10^{-1}	-1.3796×10^{-12}	3.5385×10^{-13}	
c_5	−5.8169	-1.8684×10^{-5}	1.6484×10^{-16}	-3.966×10^{-17}	

DOI: 10.52396/JUSTC-2023-0021
JUSTC, **2023**, 53(10): 1005

$$\varepsilon_{\mathrm{m}}=\sum_{j=1}^{Jcw} a_j\left[1-\exp\left(\kappa_{p,j}p_{\mathrm{m}}S\right)\right], \tag{6}$$

where p_{m} is the pressure of the mixture, and a_j is the temperature-dependent coefficient of jth gray gas (the number of gray gas is 3, i.e., $Jcw=3$) and represents the proportion of blackbody emission in the corresponding spectral range of each gray gas:

$$a_j=\sum_{k=0}^{3} b_{j,k}T^k. \tag{7}$$

The Smith's model considers three gray gases and assumes a constant molar ratio of 2∶1 between H_2O and CO_2 in the mixture. The model parameters are listed in Table 2. However, this brings the first limitation of this model since in the combustion field, the local partial pressure of H_2O and CO_2 would vary from one point to another. Furthermore, this model relies on an old spectral database to generate the coefficients, and the study has shown that this could lead to lower accuracy compared to the new versions of HITEMP2010[13].

Cassol's WSGG-based model[15], In contrast to Smith's model, Cassol et al.[15] can account for the variations in the molar ratios between H_2O and CO_2 throughout the practical combustion field based on the newly updated spectral data of HITEMP2010. Since the WSGG correlations for soot are provided in this model, the total emissivity is calculated as follows:

$$\varepsilon_{\mathrm{m}}=\sum_{j_w=0}^{J_W}\sum_{j_c=0}^{J_c}\sum_{j_s=0}^{J_s} a_{j_m}\left[1-\exp\left(\kappa_{\mathrm{m},j_m}S\right)\right]. \tag{8}$$

For a mixture of H_2O-CO_2-soot, the temperature coefficient of each species (a_{j_m}) and the mixture absorption coefficient (κ_{m,j_m}) are determined following a probabilistic argument[16] as:

$$\begin{aligned}\kappa_{\mathrm{m},j_m}&=\kappa_{w,j_w}+\kappa_{c,j_c}+\kappa_{s,j_s},\\ a_{j_m}&=a_{w,j_w}\times a_{c,j_c}\times a_{s,j_s}.\end{aligned} \tag{9}$$

The number of gray gases considered for water, carbon dioxide, and soot in this model is 4. A previous study[17] showed that marginal effects on the accuracy were observed when the number of gray gases exceeded four. The coefficients used in this model are given in Table 3.

These five models are labeled FDS, Barlow, Cassol, WSmith, and WCassol, respectively. Overall, the former three models rely on the Planck-mean absorption coefficient to determine the medium emittance, using different databases for the curve fittings; the latter two resort to the WSGG-based correlations, and these two models are differentiated mainly by the spectral database and assumption for H_2O and CO_2 mixture molar ratio. Meanwhile, the latter four models are integrated into the FDS by the newly coded program. Their performance in the prediction of large-scale pool fires is thoroughly evaluated in a later section.

2.2 Computational setup

The effective filtered form of the transport equations for species mass fraction, momentum, and energy for a three-dimensional, transient, low Mach number compressible flow was solved in a Cartesian coordinate system[18]. The fluid is assumed to be an ideal gas, and an additional Poisson equation is introduced for the pressure-velocity coupling[19]. For the convective terms of the scalar quantities, the calculations

Table 2. Smith's WSGG correlation coefficient of the H_2O-CO_2 mixture when the ratio of the partial pressures of these two components is 2.0[14].

j	$\kappa_{p,j}\left(\mathrm{m^{-1}\cdot atm^{-1}}\right)$	$b_{j,0}$	$b_{j,1}\left(\mathrm{K^{-1}}\right)$	$b_{j,2}\left(\mathrm{K^{-2}}\right)$	$b_{j,3}\left(\mathrm{K^{-3}}\right)$
1	0.4201	6.508×10^{-1}	-5.551×10^{-4}	3.029×10^{-7}	-5.353×10^{-11}
2	6.516	-2.504×10^{-2}	6.112×10^{-4}	-3.882×10^{-7}	6.528×10^{-11}
3	131.9	2.718×10^{-1}	-3.118×10^{-4}	1.221×10^{-7}	-1.612×10^{-11}

Table 3. The coefficients for Cassol's WSGG-based model[15].

	j	$\kappa_{p,j}\left(\mathrm{m^{-1}\cdot atm^{-1}}\right)$	$b_{j,1}$	$b_{j,2}\left(\mathrm{K^{-1}}\right)$	$b_{j,3}\left(\mathrm{K^{-2}}\right)$	$b_{j,4}\left(\mathrm{K^{-3}}\right)$	$b_{j,5}\left(\mathrm{K^{-4}}\right)$
CO_2	1	0.138	9.99×10^{-2}	6.441×10^{-4}	-8.649×10^{-7}	4.127×10^{-10}	-6.774×10^{-14}
	2	1.895	9.42×10^{-3}	1.036×10^{-4}	-2.277×10^{-8}	-2.134×10^{-11}	6.497×10^{-15}
	3	13.301	1.451×10^{-4}	-3.073×10^{-4}	3.765×10^{-7}	-1.841×10^{-10}	3.016×10^{-14}
	4	340.811	-2.915×10^{-1}	2.523×10^{-4}	-2.61×10^{-7}	9.965×10^{-11}	-1.326×10^{-14}
H_2O	1	0.171	6.617×10^{-2}	5.548×10^{-4}	-4.841×10^{-7}	2.229×10^{-10}	-4.017×10^{-14}
	2	1.551	1.1045×10^{-1}	0.576×10^{-5}	2.4×10^{-7}	-1.701×10^{-10}	3.096×10^{-14}
	3	5.562	-4.915×10^{-2}	7.063×10^{-4}	-7.012×10^{-7}	2.607×10^{-10}	-3.494×10^{-14}
	4	49.159	2.3675×10^{-1}	-18.91×10^{-5}	-9.07×10^{-9}	4.082×10^{-11}	-8.778×10^{-15}
Soot	1	2875.86	1.29×10^{-3}	-5.45×10^{-5}	1.23×10^{-8}	-8.470×10^{-12}	1.6807×10^{-15}
	2	39234.90	1.2611	-3.192×10^{-3}	2.772×10^{-6}	-1.005×10^{-9}	1.3280×10^{-13}
	3	160748.00	-2.576×10^{-1}	3.621×10^{-3}	-4.012×10^{-6}	1.549×10^{-9}	-2.078×10^{-13}
	4	495898.00	7.98×10^{-2}	-7.208×10^{-4}	1.587×10^{-6}	-7.089×10^{-10}	9.769×10^{-14}

DOI: 10.52396/JUSTC-2023-0021
JUSTC, **2023**, 53(10): 1005

are performed using the CHARM (cubic/parabolic high-accuracy resolution method) in the second-order accuracy TVD (total variation diminishing) format. A low-pass box filter with width proportional to the grid cell size is used for LES spatial filtering, and turbulence closure is achieved using a Deardorff eddy viscosity model for the Navier–Stokes equations and standard gradient assumptions for species and energy transport, assuming a constant Pr and Sc number of 0.5. In addition, for the stability of the calculations, the time step is limited by the use of the CFL number and the Von Neumann constraint, which range from 0.8 to 1. Combustion is modeled based on mixing-controlled, single-step, and infinitely fast chemical reactions[10]. A fixed proportion of the consumed mass of fuel determines soot production.

A simple pyrolysis model is used to simulate fuel evaporation by specifying a constant mass loss rate per unit area. According to the experiments, the pool has a diameter of 1 m and a depth of 0.15 m. The distance between the liquid surface and the pool's edge is maintained at 1 cm. It was found[20] that the mass loss rate of methanol fuel ($\dot{m}''$) is related to the ratio of the heat of combustion (Δh_c) and the heat of gasification (Δh_g):

$$\begin{aligned} \dot{m}'' &= \theta \frac{\Delta h_c}{\Delta h_g}, \\ \Delta h_g &= \Delta h_v + \int_{T_0}^{T_b} c_p \mathrm{d}T, \end{aligned} \tag{10}$$

where the smoke production rate θ is set to 0.001, so the resulting $\dot{m}''$ is 0.019. In addition, the grid cell size dx has a significant impact on the simulation calculation. In general, the numerical error decreases with increasing D^*/dx, while the flame characteristic diameter D^* is a function of the total heat release rate ($\dot{Q}$):

$$D^* = \left(\frac{\dot{Q}}{\rho_\infty C_P T_\infty \sqrt{g}} \right)^{\frac{2}{5}}, \tag{11}$$

Here, ρ_∞ denotes the ambient density, C_P denotes the specific heat of air, T_∞ denotes the ambient temperature, and g is the gravitational acceleration. It is shown that the simulation results are in good agreement with the experiments when the grid size is taken between [$D^*/16$, $D^*/4$][10]. Following this criterion, in this work, unless otherwise specified, the calculations are performed using a 1 cm grid with a computational domain of 3.2 m×1.2 m×2.4 m, as schematically shown in Fig. 1. The total calculation time is 30 s, and since the results vary with the time series, all the results are averaged over 10 –20 s, during which the combustion reaches a stable stage, and the combustion rate reaches a predetermined value.

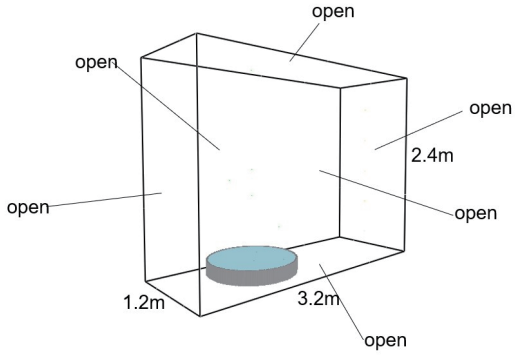

Fig. 1. Schematic diagram of the computational domain.

2.3 Verification of the models

It is necessary to verify the correctness of the new code before the calculation of the complex turbulent fire combustion, so this subsection first presents the results of the radiation computation for the domain between two infinitely long flat plates (i.e., the plate height is 12.5 times the plate spacing)[21]. This configuration can be assumed to be a quasi-one-dimensional, steady-state heat transfer problem, ignoring the effect of complex flow and thus providing reliable data for comparing and validating the model[22–24]. A grid of 200 cells is used along the x-direction (i.e., the direction of plate spacing), and the y-direction (i.e., the plate height direction) is discretized into 63 grid cells. Forty-eight control angles are used for the angular discretization in the RTE equation. In the x-direction, the initial molar concentrations of components H_2O and CO_2, the volume concentration of soot, and the temperature are given:

$$T(x) = 400 + 1400\sin^2(2\pi x), \tag{12}$$

$$Y(x) = Y_{\max}\sin^2(2\pi x), \tag{13}$$

where the Y_{max} value for H_2O is 0.2 and the Y_{max} of CO_2 is 0.1. The Y_{max} value for carbon fume is 10^{-5}. Fig. 2 shows the radiation heat source S_{radi} predicted from the four newly coded models (i.e., Barlow, Cassol, WSmith, and WCassol) in comparison to the one calculated in previous Ref. [25]. The local error associated with the FDS computations is defined as $\delta = \left|S_{\text{radi}}^{\text{FDS}} - S_{\text{radi}}^{\text{ref}}\right| / \max\left(\left|S_{\text{radi}}^{\text{FDS}}\right|\right)$. It can be seen that these four models coupled into FDS agree well with the literature results, along with a maximum error of no more than 3.5%. These results verify the correctness of the models and imply that the modified FDS code can provide reliable predictions for later discussion.

3 Results and discussion

3.1 Centerline gas temperature

The gas temperature along the centerline of the pool fire is shown in Fig. 3. The measured maximum temperature is located approximately 0.3 m above the burner exit. This position of peak temperature was better predicted by four other models except for the Barlow model, which peaks the temperature at approximately 0.2 m. In comparison to the experimental value of 1370 K,

The peak temperature predicted by Barlow and FDS is 1301.39 K and 1316.67 K, with errors of 5% and 3.8%, respectively. The errors are higher than those calculated by the other three models, with an error of almost 3%. The experiments show that the temperature profile changes steeply near the fuel surface, and all five radiation models reproduce this trend well. The gas temperature at 0.05 m above the burner is approximately (1144 ± 424) K. In general, compared with the

DOI: 10.52396/JUSTC-2023-0021
JUSTC, **2023**, 53(10): 1005

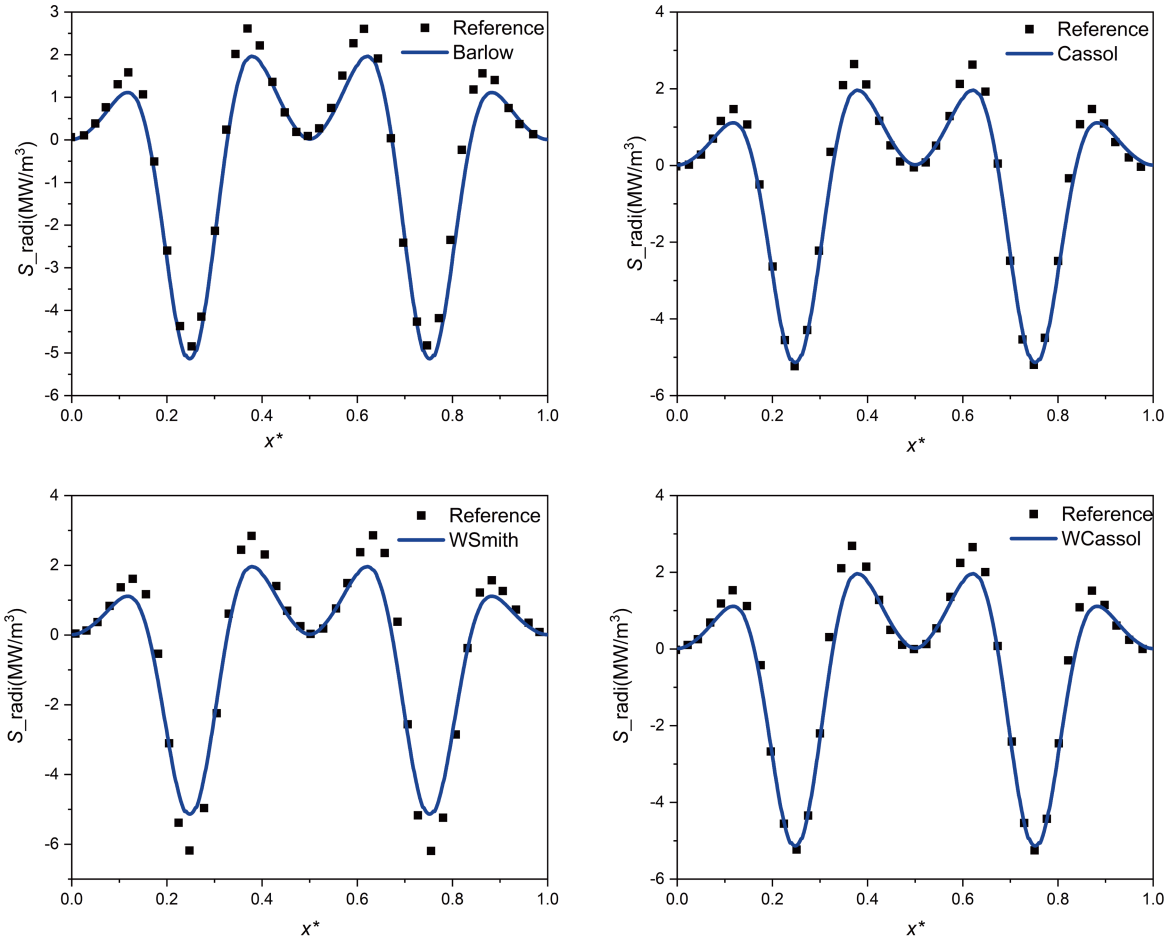

Fig. 2. Validation of the results of 1D RTE calculations for the newly coupled radiation models.

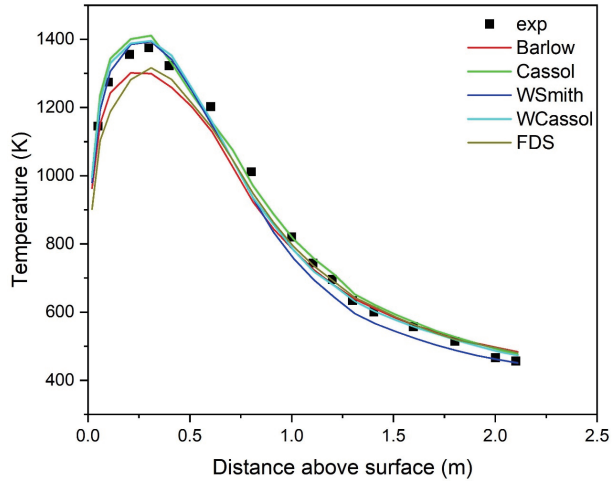

Fig. 3. Temperature distribution along the central axis of the pool fire.

default FDS and the Barlow models, the other three models are in better agreement with the experiments, especially in the range of Z<0.6 m. Moreover, WCassol performs best given that the underestimation of temperature in the downstream region is observed for the WSmith model. This result indicates that when the WSGG-based model is adopted, the variation in the concentration ratio of the local components (H_2O and CO_2) in the medium emittance calculation should have an important impact on the accuracy of radiation prediction. Meanwhile, since the Cassol model, relying on the Planck-mean absorption coefficient, also shows superiority to the default FDS and Barlow models, the spectral database may play an important role in radiation calculation. Among all the radiation models, the Cassol and WCassol models appear to be the best candidates for present flame computation. This can be attributed to the same database of HITEMP2010 that both models used. The high temperature during combustion causes gas particles to acquire higher energy, and therefore, the spectral lines resulting from jumps between higher energy levels, commonly known as hot lines, appear in the spectrum. The coefficients of the Barlow model are derived from the narrow band model of the database RADCAL, and the database of the WSmith model is an out-of-date version of HITEMP, both of which do not contain information on the spectral properties of hot lines in the high-temperature range.

3.2 Pulsation frequency

Pool fires always exhibit periodic pulsation behavior. The flame pulsation frequency is one of the fundamental and essential parameters of pool fires, which can help to understand the buoyancy effect and its interaction with the structure of combustion and annular vortex[26]. The interaction between the vertical structure of combustion and the annular vortex

DOI: 10.52396/JUSTC-2023-0021
JUSTC, **2023**, 53(10): 1005

dominates the flow field[27]. In previous studies, the pulsation frequency of pool fires has been measured based on the fluctuating frequency of flame thermal radiation, the frequency of smoke buoyancy or vortex shedding, and the variation in flame height[28]. This work calculates the pulsation phenomenon through the dynamics of vertical velocity. The instantaneous vertical velocity is extracted at the positions of x = 0 m and y = 0.505 m by referring to the experimental work of Tieszen et al.[29] using PIV to measure the flow field. The Fourier fast transform (FFT) was used to convert the time series of vertical velocity data into a function of frequency and amplitude. Since the time series started from 0 s, a high-pass FFT was performed to eliminate the right-angle offset before the FFT. The pulsation periods obtained for the different radiation models are shown in Fig. 4. The pulsation period of flame height measured in the NIST experiment using the camera is 1.37 Hz, which is comparable to the model prediction of a value of approximately (1.37 ± 0.04) Hz. Generally, good agreement is observed. The result of the Cassol model is closer to the experiment.

3.3 Instantaneous distribution of the flame characteristics

Snapshots of the velocity vector, temperature, radiation heat flux (Q_r), absorption coefficient κ_m, and species mole fraction (X_{H_2O}, X_{CO_2}) calculated using different radiation models are shown in Fig. 5. The radiation heat flux is determined by:

$$-\nabla\cdot Q_r''(x)(\text{gas}) = \kappa(x)[U(x) - 4\pi I_b(x)],$$
$$U(x) = \int_{4\pi} I(x, s')\,\mathrm{d}s'. \tag{14}$$

The instantaneous velocity vector field is also colored by the local fuel methanol concentration. The velocity field is highly consistent with the gradient of the temperature field. Close to the burner (Z<0.5 m), the flow is more turbulent with strong mixing, and the temperature rises quickly to the peak value (see Fig. 3). When moving downstream, turbulence is weak, and the temperature and density gradients become more considerable, causing a larger-scale vortex structure. Comparatively, the differences in the temperatures predicted by different models are less pronounced than those shown for the radiative heat flux (Q_r). Meanwhile, the intense radiation region seems less correlated to the high-temperature domain, especially downstream. The distribution of combustion products of X_{H_2O} and X_{CO_2} could explain this. According to Ref. [30], the radiation intensity is generally a function of the fourth power of temperature and the medium emittance. Therefore, the concentration of radiative species that determines the mixture absorption coefficient also plays a critical role in the distribution of Q_r. Furthermore, by comparing X_{H_2O}, X_{CO_2}, and Q_r, the species of water appears to be more dominant in the correlations with Q_r in the present flame.

In addition, theoretically or in cases of laminar conditions, the high-temperature region usually overlaps with the area featuring a high concentration of primary products, i.e., H_2O and CO_2. However, in turbulent pool fires, the displacement between temperature and concentration maxima would be induced because of buoyancy and air-entrainment effects, and the region of elevated product concentration tends to present near the pool surface. Thus, the present results also indicate that for pool fires, the evaluation of radiation characteristics should consider both the distribution of temperature and the species concentration.

The normalized absorption coefficient of $\kappa_p = \kappa_m/\kappa_{max}$ is also shown in the Fig. 5. κ_{max} is the maximum absorption coefficient predicted by different models and is shown in Table 4. For the models based on the Planck average absorption coefficient, Cassol's maximum is two orders of magnitude smaller than that of Barlow and FDS. In contrast, the WSmith and WCassol models do not differ much.

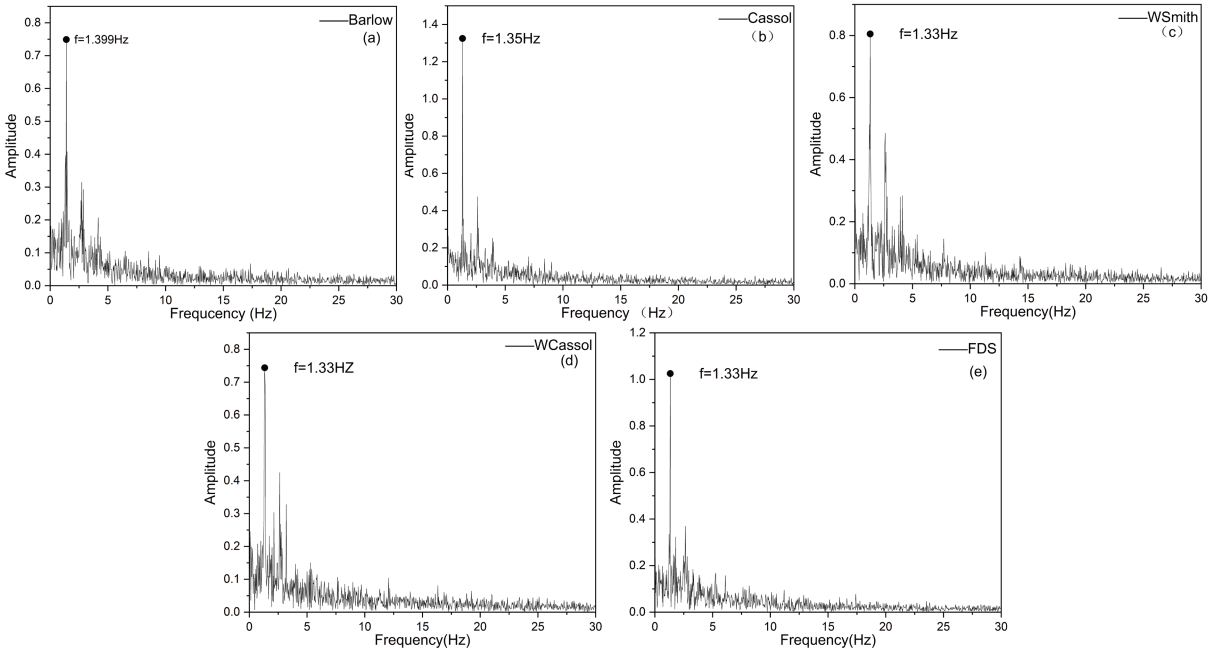

Fig. 4. Frequency amplitude plots of velocities under different radiation models: (a) Barlow model, (b) Cassol model, (c) WSmith model, (d) WCassol model, and (e) FDS model, respectively.

DOI: 10.52396/JUSTC-2023-0021
JUSTC, **2023**, 53(10): 1005

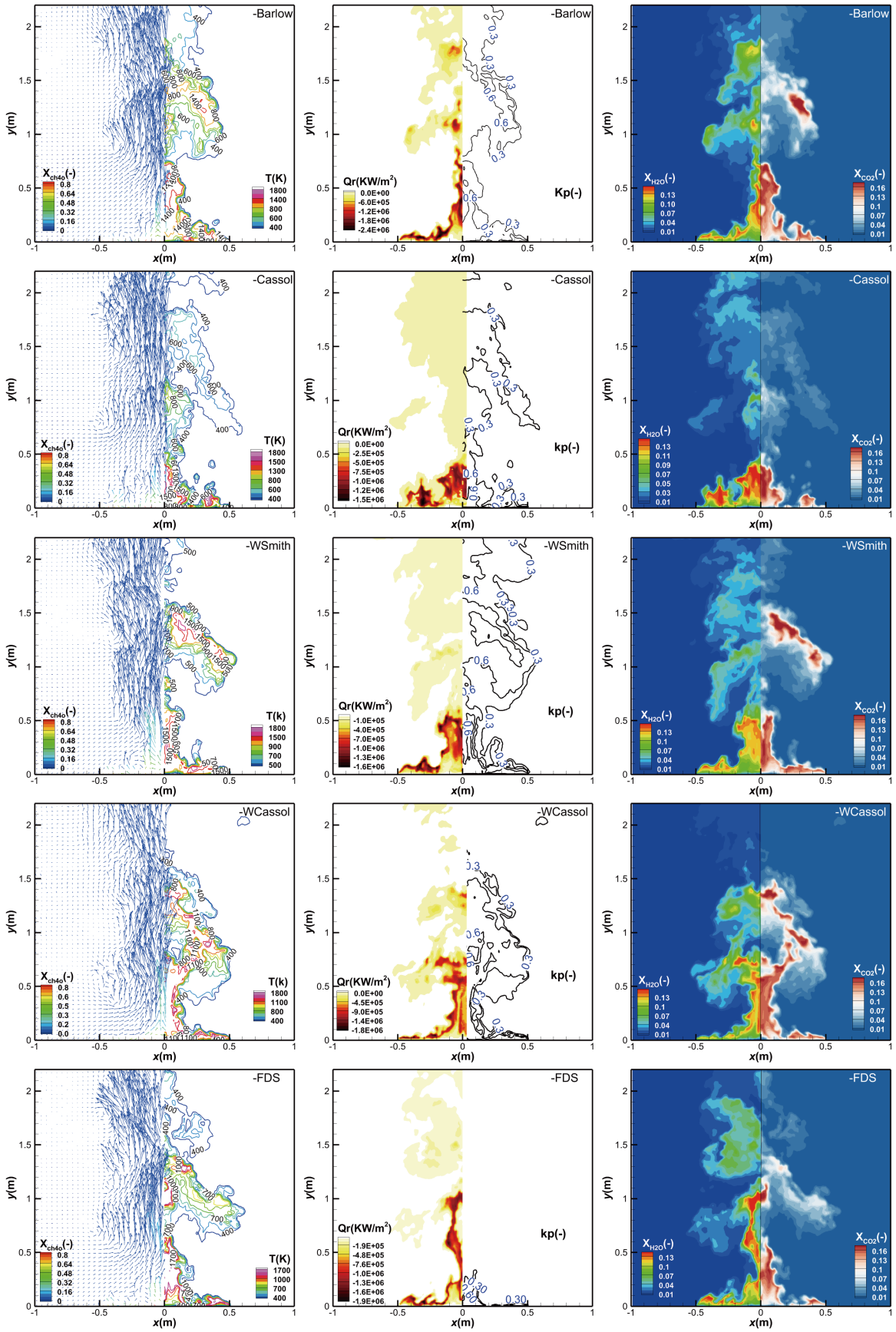

Fig. 5. Transient velocity vector, temperature, radiation heat flux (Q_r), absorption coefficient (κ_p), and concentrations of H_2O and CO_2 predicted by different radiation models.

DOI: 10.52396/JUSTC-2023-0021
JUSTC, **2023**, 53(10): 1005

Table 4. Maximum absorption coefficients (κ_{max}) calculated by different radiation models.

Model	Barlow	Cassol	WSmith	WCassol	FDS
κ_{max}	3.3959	0.030899	1.0721	0.98704	4.5134

3.4 Radiation heat flux

The magnitude of radiation heat flux determines the hazard posed by the fire and directly affects the rate of fire spread. Fig. 6 compares the radiation heat flux calculated by the five radiation models with those obtained from the NIST measurements at 2.8 m away from the fire centerline. The Barlow model deviates from the observed values with a maximum error of 50%, followed by the WSmith model with 36%. Consistent with the temperature prediction, the WCassol model reaches the best agreement with only a 15% deviation. The default FDS model and the Cassol model share a similar prediction with the WCassol model.

For these five GG radiation models, gray gas is assumed, and the radiative properties of the participating gases are a constant value κ_m relative to the wavenumber spectrum. This simplification avoids the direct coupling of property variations over hundreds of thousands of spectral lines, but it undoubtedly leads to a decrease in accuracy. It is well known that H_2O, CO_2, and soot are the leading absorbing-emitting energy media in fire scenarios. In contrast to the two diatomic gases of H_2O and CO_2, the dependence of soot on wavenumber can often be approximately linear. Due to the fuel properties of methanol, the soot production rate is marginal. In contrast, H_2O and CO_2 become the dominant absorption medium, with a much higher spectral dependence than soot. This constitutes the main difficulty for accurately modeling the radiation in weekly soot methanol pool fires based on the GG model. Therefore, all GG radiation models used in this work underestimate the radiation heat flux. It is worth noting that the errors in measurement could also contribute partly to the discrepancy.

3.5 Computational efficiency

All LES computations are carried out using the same scenario file and a server computing system of Centos7 with two Intel® Xeon® Platinum8375C@2.99 GHz central processors with a total of 128 cores and 256 GB RAM. The information on the computational elapsed time, maximum errors in temperature and radiant heat flux Q_r, and pulsation periods for the different radiation models are presented in Table 5. The original FDS model has the highest computational efficiency, while the computational time of the WCassol model is significantly higher than that of the other radiation models. This is because the WCassol model is equivalent to the usage of 125 gray gases and thus requires additional computational power to calculate different temperature-dependent coefficients and absorption coefficients. It is worth mentioning that the calculation efficiency of the WSmith model does not differ much from that of the Barlow, FDS, and Cassol models because only the fixed component ratios and three gray gases are considered in the WSmith model. There is almost no difference in the calculation efficiency of the Barlow and Cassol models compared to the FDS model because both of them assume one gray gas. Overall, the GG model based on the Planck-averaged absorption coefficient is faster than the GG model using the WSGG-based correlations. Referring to the previous discussion, the predictions from the Cassol model and WCassol model have the best agreement with the experiments. Furthermore, if the CPU computational time is considered, the Cassol model seems to be the best choice that compromises between accuracy and efficiency. However, this conclusion should be further studied in the simulations of other complex pool fires, including strong sooting flames, which will be the focus of future work.

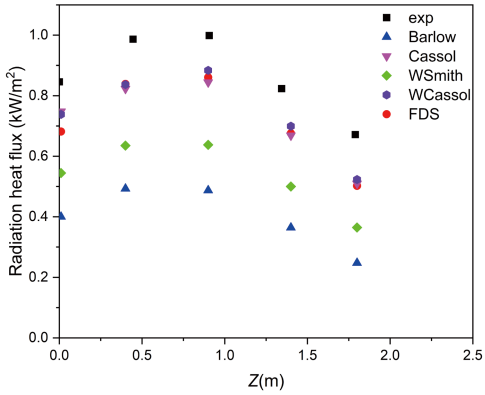

Fig. 6. Vertical distribution of radiation flux at 2.8 m from the center of the pool.

4 Conclusions

The prediction performance and accuracy of different radiation models were thoroughly evaluated in an LES of 1 m methanol pool fires. This is achieved by the modifications of the FDS source code that will then couple different gray gas radiation models, i.e., the traditional ones based on the Planck average absorption coefficient and the one relying on the WSGG-based correlations for medium emittance. The main conclusions are as follows:

(Ⅰ) The accuracy of the radiation models (WSmith and WCassol) based on the WSGG correlation is better in the temperature calculation. Although the Cassol model does not use the WSGG method to obtain the absorption coefficients, its predictions are close to those of the WSmith and WCassol models because it employs the latest spectral database HITEMP2010. In addition, both the FDS model and the Barlow model underestimate the maximum temperature value.

Table 5. Comparison of the computational performance of different radiation property models.

Model	Time (h)	Temperature error	Pulsation frequency (Hz)	Radiation heat flux error
Barlow	15.1	5%	1.399	50%
Cassol	16.8	<3%	1.35	15%
WSmith	19.5	<3%	1.33	36%
WCassol	153.5	<3%	1.33	15%
FDS	14.2	3.8%	1.33	17%

DOI: 10.52396/JUSTC-2023-0021
JUSTC, **2023**, 53(10): 1005

The pulsation period is well predicted by all radiation models.

(Ⅱ) The Cassol and WCassol models have the best accuracy among all radiation models, but the latter is computationally time-consuming. The Cassol model is concluded to be a good choice that nicely balances computational efficiency and accuracy.

This work presents a newly updated assessment of radiation modeling for large-scale pool fires and reveals the importance of both temperature and concentration distribution in accurately evaluating the radiation flux and their special correlations in pool fires. To the author's best knowledge, there is limited research on this topic. The default GG model in FDS usually underestimated the radiant heat flux when calculating low-sooty pool fires, which can affect fire hazard assessments. The new coupled model improves the accuracy of the radiation calculation, and the results also provide ideas for future study on the establishment of a suitable radiation model for other complex liquid-fueled pool fires under various fuel-type and flame-sooting conditions.

Acknowledgements

This work was supported by the National Natural Science Foundation of China (52006151), the National Key R&D Program of China (2022YFC3003100), and the Civil Aircraft Scientific Research Project of the Industry and Information Technology (BB2320000045, DD2320009001).

Conflict of interest

The authors declare that they have no conflict of interest.

Biographies

Qianjun Zhou is a master of science at the University of Science and Technology of China. His research interest includes CFD, radiation modeling in fire simulation, and spectral modeling.

Yong Hu is currently a Researcher at the University of Science and Technology of China. He received his Ph.D. degree in Physical Chemistry from the University of Heidelberg, Germany. His research interests include large-scale computation, high-precision model construction, simulation of fire combustion dynamics evolution, intelligent prediction, and machine learning.

Yong Jiang is a Professor at the University of Science and Technology of China (USTC). He received his Ph.D. degree in Engineering in 1998. Afterwards, he worked as a postdoctoral fellow at USTC. His research interests include computer simulation, modeling, and precision measurement techniques of fire and combustion.

References

[1] Abdolhamidzadeh B, Abbasi T, Rashtchian D, et al. Domino effect in process-industry accidents —An inventory of past events and identification of some patterns. *Journal of Loss Prevention in the Process Industries,* **2011**, *24*: 575–593.

[2] Fang J, Wang J, Tu R, et al. Optical thickness of emissivity for pool fire radiation. *International Journal of Thermal Sciences,* **2018**, *124*: 338–343.

[3] Sacadura J F. Radiative heat transfer in fire safety science. *Journal of Quantitative Spectroscopy and Radiative Transfer,* **2005**, *93*: 5–24.

[4] Yao Y, Li Y Z, Ingason H, et al. Scale effect of mass loss rates for pool fires in an open environment and in tunnels with wind. *Fire Safety Journal,* **2019**, *105*: 41–50.

[5] Fernandes C S, Fraga G C, França F H R, et al. Radiative transfer calculations in fire simulations: An assessment of different gray gas models using the software FDS. *Fire Safety Journal,* **2021**, *120*: 103103.

[6] Barlow R S, Karpetis A N, Frank J H, et al. Scalar profiles and NO formation in laminar opposed-flow partially premixed methane/air flames. *Combustion and Flame,* **2001**, *127*: 2102–2118.

[7] Cassol F, Brittes R, Centeno F R, et al. Evaluation of the gray gas model to compute radiative transfer in non-isothermal, non-homogeneous participating medium containing CO_2, H_2O, and soot. *Journal of the Brazilian Society of Mechanical Sciences and Engineering,* **2015**, *37*: 163–172.

[8] Hostikka S, Mcgrattan K, Hamins A. Numerical modeling of pool fires using les and finite volume method for radiation. *Fire Safety Science,* **2003**, *7*: 383–394.

[9] Krishnamoorthy G, Borodai S, Rawat R, et al. Numerical modeling of radiative heat transfer in pool fire simulations. In: Proceedings of ASME 2005 International Mechanical Engineering Congress and Exposition. Orlando, Florida, USA: ASME, **2008**: 327–337.

[10] McGrattan K, McDermott R, Weinschenk C, et al. Fire Dynamics Simulator Users Guide, Sixth Edition, Special Publication (NIST SP). Gaithersburg, MD, USA: National Institute of Standards and Technology, **2013**.

[11] Sung K, Chen J, Bundy M, et al. The characteristics of a 1 m methanol pool fire. *Fire Safety Journal,* **2021**, *120*: 103121.

[12] Grosshandler W L. Radcal: A Narrow-Band Model for Radiation Calculations in a Combustion Environment. Washington, DC: NIST, **2018**.

[13] Rothman L S, Gordon I E, Barber R J, et al. HITEMP, the high-temperature molecular spectroscopic database. *Journal of Quantitative Spectroscopy and Radiative Transfer,* **2010**, *111*: 2139–2150.

[14] Smith T F, Shen Z F, Friedman J N. Evaluation of coefficients for the weighted sum of gray gases model. *Journal of Heat Transfer,* **1982**, *104*: 602–608.

[15] Cassol F, Brittes R, França F H R, et al. Application of the weighted-sum-of-gray-gases model for media composed of arbitrary concentrations of H_2O, CO_2 and soot. *International Journal of Heat and Mass Transfer,* **2014**, *79*: 796–806.

[16] Denison M K, Webb B W. The spectral-line weighted-sum-of-gray-gases model for H_2O/CO_2 mixtures. *Journal of Heat Transfer,* **1995**, *117*: 788–792.

[17] Johansson N, Ekholm M. Variation in results due to user effects in a simulation with FDS. *Fire Technology,* **2018**, *54*: 97–116.

[18] McGrattan K, Hostikka S, McDermott R, et al. Fire Dynamics Simulator Technical Reference Guide Volume 1: Mathematical Model. Washington, DC: NIST, **2013**.

[19] Rehm R G, Baum H R. The equations of motion for thermally driven, buoyant flows. *Journal of Research of the National Bureau of Standards,* **1978**, *83*: 297.

[20] Gottuk D T, White D A. Liquid fuel fires. In: Hurley M J, editor. SFPE Handbook of Fire Protection Engineering. New York: Springer, **2016**: 2552−2590.

[21] Fraga G C, Zannoni L, Centeno F R, et al. Evaluation of different gray gas formulations against line-by-line calculations in two- and three-dimensional configurations for participating media composed

DOI: 10.52396/JUSTC-2023-0021
JUSTC, **2023**, 53(10): 1005

by CO_2, H_2O and soot. *Fire Safety Journal,* **2019**, *108*: 102843.

[22] Dorigon L J, Duciak G, Brittes R, et al. WSGG correlations based on HITEMP2010 for computation of thermal radiation in non-isothermal, non-homogeneous H_2O/CO_2 mixtures. *International Journal of Heat and Mass Transfer,* **2013**, *64*: 863–873.

[23] Coelho F R, França F H R. WSGG correlations based on HITEMP2010 for gas mixtures of H_2O and CO_2 in high total pressure conditions. *International Journal of Heat and Mass Transfer,* **2018**, *127*: 105–114.

[24] Xu J, Chen R, Meng H. WSGG models for radiative heat transfer calculations in hydrogen and hydrogen-mixture flames at various pressures. *International Journal of Hydrogen Energy,* **2021**, *46*: 31452–31466.

[25] da Fonseca R J C, Fraga G C, da Silva R B, et al. Application of the WSGG model to solve the radiative transfer in gaseous systems with nongray boundaries. *Journal of Heat Transfer,* **2018**, *140*: 052701.

[26] Hu L, Hu J, de Ris J L. Flame necking-in and instability characterization in small and medium pool fires with different lip heights. *Combustion and Flame,* **2015**, *162*: 1095–1103.

[27] Bejan A. Predicting the pool fire vortex shedding frequency. *Journal of Heat Transfer,* **1991**, *113*: 261–263.

[28] Chen X, Lu S, Wang X, et al. Pulsation behavior of pool fires in a confined compartment with a horizontal opening. *Fire Technology,* **2016**, *52*: 515–531.

[29] Tieszen S R, O'Hern T J, Schefer R W, et al. Experimental study of the flow field in and around a one meter diameter methane fire. *Combustion and Flame,* **2002**, *129*: 378–391.

[30] Hottel H C, Sarofim A F. Radiative Transfer. New York: McGraw-hill Book Company, **1967**.

DOI: 10.52396/JUSTC-2023-0021
JUSTC, **2023**, 53(10): 1005